Journal of Statistical Physics, Vol. 69, Nos. 3/4, 1992

The Critical Behavior of Dimer–Dimer Surface Reaction Models. Monte Carlo and Finite-Size Scaling Investigation

Ezequiel V. Albano[1]

Received October 30, 1991; final May 22, 1992

Two models based upon the well-known mechanism for the oxidation of hydrogen on transition metal surfaces, which may also apply to generic dimer–dimer surface reaction processes of the type $(1/2)\,A_2 + B_2 \rightarrow B_2A$, are proposed and studied on the square lattice of side L ($L \leqslant 600$) by means of Monte Carlo simulations and finite-size analysis. Both models exhibit irreversible (kinetic) phase transitions (IPT) from a reactive state with sustained production of B_2A molecules to off-equilibrium surface poisoned states with the reactants, i.e., without production. The location of the critical points at which the IPTs take place in the $L = \infty$ limit is determined by means of a finite-size scaling analysis. Also, it is shown that at criticality some relevant quantities, such as the rate of B_2A production and the coverage with the reactants, exhibit simple power-law behavior, which allow us to determine the corresponding critical exponents.

KEY WORDS: Irreversible phase transitions; critical behavior; heterogeneous catalysis.

1. INTRODUCTION

Heterogeneous catalysis is a chemical reaction at the interface of two phases, for example, at the gas–solid interface. The chemical reaction at the catalyst proceeds at a higher rate than in the homogeneous phase, i.e., the gas phase without the catalyst. The elementary steps in a heterogeneously catalyzed reaction are in principle well known. These involve adsorption, migration of adsorbed particles, chemical reactions, and desorption of the products. This kind of catalyzed reaction is essential for a great variety of

[1] Instituto de Investigaciones Fisicoquímicas Teóricas y Aplicadas, (INIFTA), Facultad de Ciencias Exactas, Universidad Nacional de La Plata, Suc. 4, C.C. 16, (1900) La Plata, Argentina.

822/69/3-4-13

technological processes and accounts for the major fraction of overall chemical production. In addition to the huge experimental effort devoted to the study of catalyzed reactions,[1] theoretical studies have also attracted considerable attention.[2] More recently the investigation of microscopic models has aroused growing interest.[2–27] One example is the study of the monomer–monomer (MM) surface reaction process of the type $A + B \to AB$,[4–10] where both reactants require a single adsorption site. It is known that if the mole fraction of B (p_B) in the gas phase is $p_B < 1/2$ ($p_B > 1/2$) the catalyst surface becomes poisoned, i.e., saturated, with A (B) species, respectively. Consequently, the MM reaction process has a single critical point at $p_B = 1/2$.[4–10] Variants of this simple MM picture exhibiting self-sustained oscillations, bistability, and chaotic behavior have been also analyzed.[6,7]

Another interesting example is the dimer–monomer (DM) surface reaction process, of the type $(1/2)A_2 + B \to BA$,[11–27] where a dimer adsorbs on a pair of neighboring empty sites while the monomer adsorbs on a single empty site. Due to the adsorption condition required by dimers, the DM process exhibits critical behavior with a finite reaction window.[11–27] In fact, for mole fraction p_B of B in the gas phase, one observes that for $p_B \leqslant p_{1B}$ ($p_B \geqslant p_{2B}$) the surface becomes poisoned with A (B) species, respectively; while for $p_{1B} < p_B < p_{2B}$ the system reaches a stationary state with AB production. So, p_{1B} and p_{2B} are critical values of p_B at which irreversible phase transitions (IPTs) from poisoned states to the stationary regime take place.[11–27] The values of both p_{1B} and p_{2B} depend on the substratum as well as on the simulation technique,[11–27] so for a review of critical values see ref. 28. The DM surface reaction model, as proposed by Ziff *et al.*,[11] has been studied by means of different techniques, such as Monte Carlo simulations,[11,13,15,17–19,22–25] the cellular automata method,[14] mean field[16,21] and Bethe–Peierls approximations,[16] the complete graph method,[9,20] the finite-size scaling approach,[22,23] etc; and on different kind of substrata, including the square lattice,[11,13,15,17–19] disordered (fractal) media,[22–25] and one-dimensional rings and strips.[13] Variants of the DM model, including the effect of variable reaction and adsorption rates,[17,20,21,26,27] diffusion,[16,17,19,28] desorption,[16,17] etc., have also been studied.

Within this context, the aim of the present work is to propose a dimer–dimer (DD) surface reaction model and to report a detailed study of two variants of such a model (details of the DD reaction schemes are described in Section 2). The discussed models, inspired by the catalytic

[2] See, e.g., the articles in *Journal of Statistical Physics*, volume 42(1/2) (1986), which provides an overview of recent progress in chemical kinetics.

oxidation of hydrogen, exhibit IPTs and their critical behavior is studied by means of Monte Carlo and finite-size scaling techniques. These methods allow us to determine the critical points as well as the relevant critical exponents. The paper is organized as follows: in Section 2 the DD surface reaction scheme is proposed and the assumptions involved are discussed; Section 3 is devoted to the description of the Monte Carlo method and simulation details. In Section 4 the results are presented and discussed. The conclusions are outlined in Section 5.

2. THE DIMER–DIMER SURFACE REACTION MODELS

The reaction scheme is based upon the well-known Langmuir–Hinshelwood (LH) mechanism, i.e., the reactants have to be adsorbed on the catalytic surface, so

$$A_2(g) + 2(*) \longrightarrow 2A(a) \tag{1a}$$

$$B_2(g) + 2(*) \underset{k_2}{\overset{k_1}{\rightleftharpoons}} 2B(a) \tag{1b}$$

$$A(a) + B(a) \longrightarrow AB(a) + (*) \tag{1c}$$

$$AB(a) + B(a) \longrightarrow B_2A(g) + 2(*) \tag{1d}$$

$$AB(a) + AB(a) \longrightarrow B_2A(g) + B(a) + (*) \tag{1e}$$

where $(*)$ denotes a vacant site on the catalyst surface, while (a) and (g) refer to the adsorbed and gas phases, respectively. Also, k_1 and k_2 are rate constants for B_2 adsorption and desorption, respectively.

It should be mentioned that the aim of the present work is to simulate generic DD reaction models based on the LH mechanism, rather than to study any actual catalytic reaction. Nevertheless, one has to recognized that the reaction scheme given by Eqs. (1a)–(1e) is inspired by the catalytic oxidation of hydrogen, i.e., $A_2 \equiv O_2$, $B_2 \equiv H_2$, $B_2A \equiv H_2O$, and $AB \equiv OH$. This reaction has been studied extensively since Faraday in the last century[29] (for reviews up to 1980–1982 see refs. 30 and 31, and for more recent results see refs. 32–35 and references therein).

As already mentioned, two variants of the reaction scheme are studied. The first one, say M1, assumes $k_1 = p_{B_2}$, where p_{B_2} is the mole fraction of B_2 in the gas phase, and $k_2 = 0$; while the second one, say M2, assumes $k_1 = p_{B_2}$ and $k_2 = \infty$. In other words, M1 assumes the irreversible adsorption of B_2 dimers, while, on the contrary, M2 considers B_2 desorption as a product of the recombinative reaction between $B(a)$ species. Notice that $k_2 = \infty$ is used to symbolize that the recombination of $B(a)$ monomers adsorbed on two NN sites occurs with probability one. Consequently,

every B_2 which does not react on adsorption is desorbed. In both cases surface diffusion of $B(a)$ species is considered. These assumptions are motivated by the fact that H atoms and H_2 molecules are more mobile and desorb at lower temperature than do O and O_2,[32–34] respectively. It should be noticed that in spite of the fact that models involving surface diffusion of the reactants are "more realistic," the influence of diffusion on the critical behavior of the system is usually not relevant, in agreement with results obtained by studying the DM surface reaction scheme.[16,17,19,28] Furthermore, Eq. (1d) corresponds to the formation of water from the recombination of hydroxyl groups, which is relevant in the actual catalytic reaction at low temperature.[33,34] Models more suitable to the high-temperature regime of the process when the step described by Eq. (1e) can be neglected also exhibit critical behavior and will be discussed in a forthcoming work.[36] Accumulation of the product on the surface can be neglected since water desorbs immediately after formation.[32–34] Also, it is assumed that the formation of an $AB(a)$ species leaves a vacant site on the surface [Eq. (1c)], based on the fact that hydroxyl groups are adsorbed through the O atom with the H pointing away or slightly tilted.[31,35]

Finally, for second-order IPTs such as those exhibited by models M1 and M2 (see below), by assuming reversible adsorption–desorption processes for both reactants simultaneously, one prevents the formation of truly saturated catalyst surfaces and consequently IPTs are no longer observed. This is in contrast to the case of first-order IPTs, where for low desorption rates one observes the existence of "effectively poisoned" states and the transition-like behavior remains.[16,37,38]

3. THE MONTE CARLO ALGORITHM AND SIMULATION DETAILS

The models are simulated on a square lattice of side L ($L \leqslant 600$) using periodic boundary conditions. Let us first describe the Monte Carlo algorithm corresponding to model M1. Initially a site, say site 1, of the catalytic surface is selected at random. Then one proceeds as follows: (i) If site 1 is occupied by an $A(a)$ species, the trial ends; (ii) If site 1 is empty, a nearest neighbor (NN) site, say site 2, is also selected at random. If site 2 is occupied, the trial ends because there is no place for dimer adsorption. Otherwise, if site 2 is also empty, a dimer, either A_2 or B_2, has to be adsorbed. So a B_2 (A_2) is selected at random with probability p_{B_2} ($1-p_{B_2}$), where p_{B_2} is the mole fraction of B_2 in the gas phase. When a dimer becomes adsorbed one has to investigate its six NN sites in order to account for the reactions described by Eqs. (1c)–(1e). These reactions are assumed to take place only when the involved species are adsorbed on NN

sites. Finally, (iii) if site 1 is occupied by a B(a), an NN site, say again site 2, is selected at random. If site 2 is occupied, the trial ends, otherwise the B(a) species is allowed to diffuse from site 1 to site 2. After that, one has to investigate three NN sites of site 2 (site 1 is now vacant!) in order to account for a possible reaction event, as described above in (ii). Since model M2 involves B_2 desorption, either after the adsorption of a B_2 dimer or after the diffusion of a B(a) species one also has to account for Eq. (1b) with $k_2 = \infty$.

Further assumptions involved in the employed algorithms are the following: AB species are formed on the site occupied by A(a) while the site corresponding to B(a) is vacated. When more than one NN of type B(a) are found around a newly adsorbed species of type A, one of them is selected at random in order to form an AB(a) species, but this intermediate immediately reacts with one (randomly selected) of the remaining B(a) to form $B_2A(g)$. Note that random selection of the B(a) species is only relevant when the number of NNs is three. On the other hand, for a newly adsorbed B species, there could be both A(a) and AB(a) NNs. If all NNs are of the same kind, the reaction is decided at random. Otherwise, if one has NNs of different type, the formation of the product $B_2A(g)$ takes precedence over the formation of the intermediate AB(a). For algorithmic convenience, simulations employ a fixed (unit) diffusion rate.

These algorithms are run into the long-time regime, monitoring the rate of B_2A production R and the surface coverages ϑ_A, ϑ_B, and ϑ_{AB} with the reactants A and B and the intermediate product AB, respectively. A Monte Carlo time unit t involves L^2 trials, so each site of the lattice may be visited once, on the average. Simulations are performed until $t = 10^4$–10^5 and averages are taken after elapsing a suitable interval of time (usually $t = 5 \times 10^3$) in order to avoid correlations with the transient period of the reaction.

Notice that in principle, both models have a single parameter, namely p_{B_2}. Nevertheless, in order to obtain reliable conclusions from Monte Carlo simulations it is essential to investigate the dependence of the results on the system size. So, results obtained with lattices of different sides ($L \leqslant 600$) are compared and finite-size scaling analysis has to be made in order to evaluate the critical points.

The simulations are performed in a multitransputer system with five T800 processors, hosted by a PC, working in parallel. The algorithms are written in OCCAM 2,[39] including a random number generator[40] which has successfully been tested in previous work (see, for example, ref. 41).

4. RESULTS AND DISCUSSION

4.1. Dependence of the Rate of Production and the Coverages on p_{B_2}

Figure 1 shows the dependence of the rate of B_2A production R and the surface coverages with the different adsorbed species on p_{B_2}, for the model M1. The existence of two IPTs at the critical values of p_{B_2} given by $p_{1B_2} \cong 0.454$ and $p_{2B_2} \cong 0.623$ ($L = 200$) can easily be observed. In fact, for $p_{B_2} \leqslant p_{1B_2}$ ($p_{B_2} \geqslant p_{2B_2}$) the production of B_2A stops irreversibly and the surface becomes always saturated (poisoned) by a binary compound formed by A(a) and AB(a) species [B(a) species], respectively. Therefore, a stationary state with sustained production of B_2A is only observed within a reaction window in the interval $p_{1B_2} < p_{B_2} < p_{2B_2}$. So, at the critical points p_{1B_2} and p_{2B_2} two IPTs from saturated states of the system to a steady-state regime with B_2A production take place. In the limit $p_{B_2} = 0$ the catalytic surface becomes saturated with A(a) only and the coverage is close to $\vartheta_A \cong 0.91$. In fact, the surface cannot completely be covered by A(a) species, because of the geometric restrictions imposed by the dimer adsorption process. Therefore, at this limit the model is similar to the random dimer filling problem (RDFP). Notice that the best estimate of the occupancy probability p_0 of the RDFP is given by $p_0 \cong 0.907$,[42,43] in excellent agreement with the result obtained for the coverage with A(a)

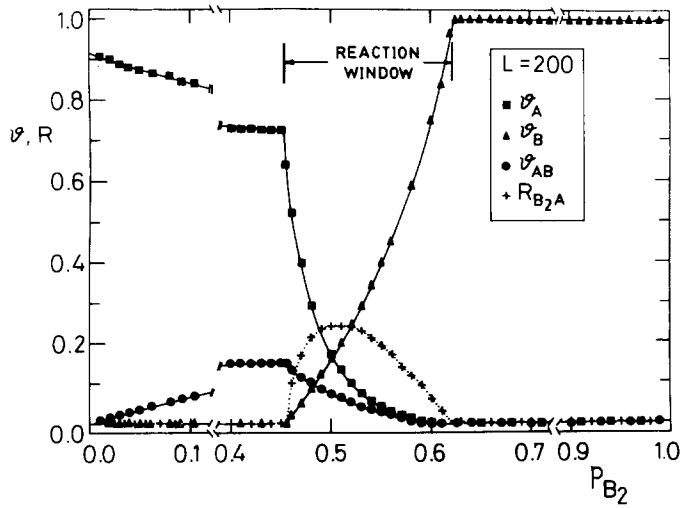

Fig. 1. Plot of the rate of B_2A production R and the surface coverages with the reactants versus p_{B_2} for the model M1. Lattice size $L = 200$. More details in the text.

species. Also, for $p_{B_2} \leqslant p_{1B_2}$ one has that the total surface coverage with the binary compound of A(a) and AB(a) species approaches $\vartheta_A + \vartheta_{AB} \cong 0.9$. For $p_{B_2} \geqslant p_{2B_2}$ one observes $\vartheta_B \cong 1$ because the geometric restrictions of the RDFP are somewhat relaxed by surface diffusion of B(a) species.

Figure 2 shows typical snapshot configurations of the reactants on the catalyst surface obtained for model M1. Just at p_{1B_2} (Fig. 2a) the surface is saturated by the binary compound formed by A(a) and AB(a) species. Only $\sim 10\%$ of the surface remains uncovered, and empty sites are always "single sites" where dimer adsorption is not possible. Upon a slight increase of p_{B_2} (Fig. 2b), rather big islands of the binary compound still account for the major fraction of the covered surface, but a few small islands of B(a) appear. For $p_{B_2} = 0.51$, i.e., just when the rate of B_2A production is maximum (Fig. 2c), the size of the islands of the binary compound is similar to

(a)

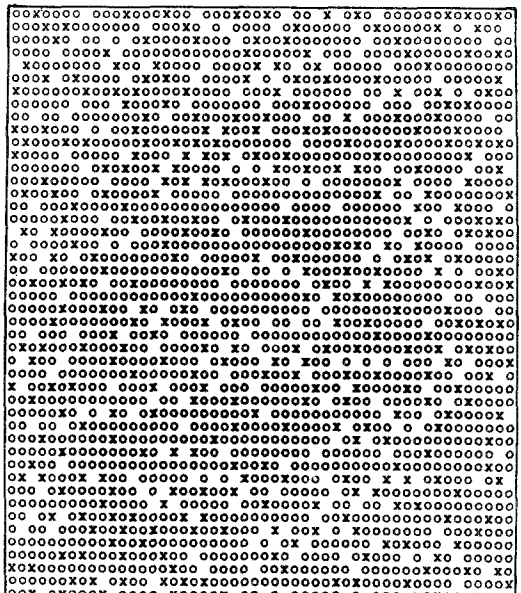

Fig. 2. Typical snapshot configurations of the reactants on the surface characteristic of the model M1. Sample size $L = 50$; (○) A(a), (■) B(a), and (×) AB(a), empty sites are left in white. (a) Saturated surface with A(a) ($\vartheta_A \cong 0.730$) and AB(a) ($\vartheta_{AB} \cong 0.154$) after $t \cong 10^3$ for $p_{B_2} = 0.4525$, i.e., just at p_{1B_2}. (b) Configuration obtained during the stationary regime for $t = 3 \times 10^3$ and slightly above p_{1B_2}, i.e., for $p_{B_2} = 0.48$, $\vartheta_A \cong 0.308$, $\vartheta_B \cong 0.063$, and $\vartheta_{AB} \cong 0.113$; (c) typical configuration obtained when R is maximum for $p_{B_2} = 0.51$ ($t = 3 \times 10^3$), $\vartheta_A \cong 0.110$, $\vartheta_B \cong 0.236$, and $\vartheta_{AB} \cong 0.056$; and (d) configuration obtained during the stationary regime ($t = 3 \times 10^3$), above the maximum of R and closer to the poisoning transition with B(a) species. $p_{B_2} = 0.54$, $\vartheta_A \cong 0.042$, $\vartheta_B \cong 0.364$, and $\vartheta_{AB} \cong 0.03$.

(b)

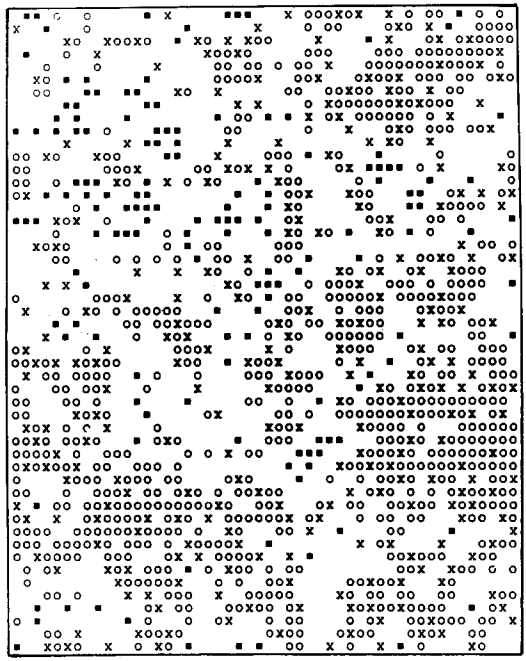

(c)

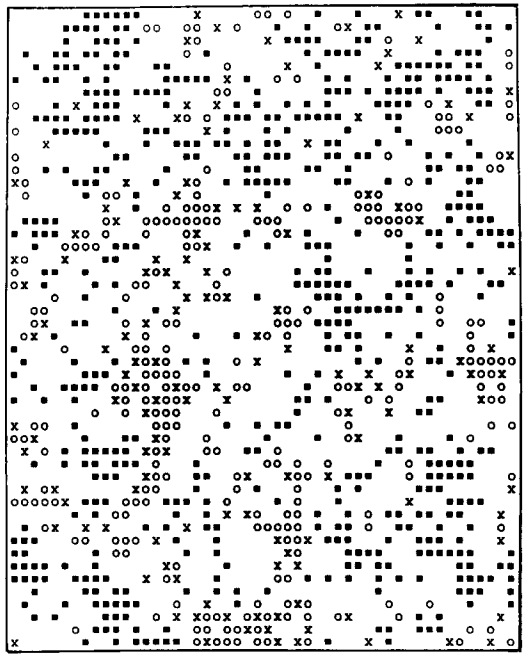

Fig. 2. (*Continued*)

(d)

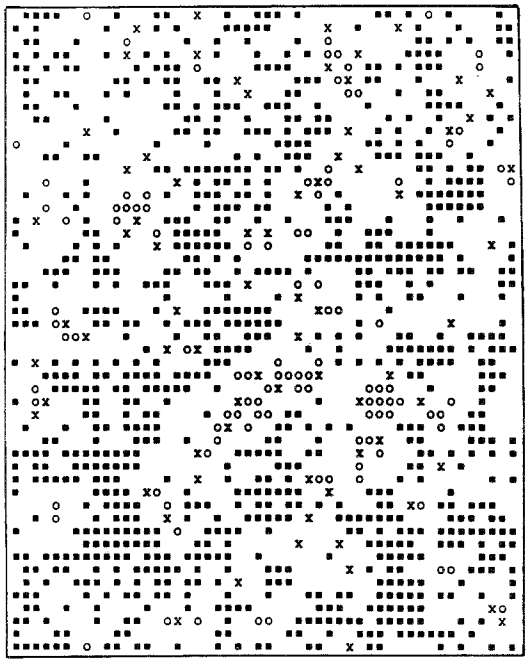

Fig. 2. (*Continued*)

that of the B(a) species ($\vartheta_A + \vartheta_{AB} \cong 0.17$ and $\vartheta_B \cong 0.24$). A further increase of p_{B_2} (Fig. 2d) causes the growth of B(a) islands, while A(a) and AB(a) are the minority species. Naturally, this trend becomes dominant on approaching p_{2B_2}.

Figure 3 shows the dependence of R, ϑ_A, ϑ_B, and ϑ_{AB} on p_{B_2} for model M2. Since this model assumes desorption of B_2 dimers as a product of the recombination reaction between B(a) species [Eq. (1b) with $k_2 = \infty$] the IPT at p_{2B_2} characteristic of M1 is no longer observed. In fact, a single IPT is observed close to $p'_{1B_2} \cong 0.476$ ($L = 200$) from a saturated state with the binary compound formed by A(a) and AB(a) species to a stationary regime with B_2A production. As discussed in the case of model M1, the total coverage of the saturated state is close to $\vartheta_A + \vartheta_{AB} \cong 0.9$.

Figure 4 shows typical snapshot configurations of the reactants on the catalyst surface obtained for model M2. Just at p'_{1B_2} (Fig. 4a) the configuration is quite similar to that already obtained with model M1 (see Fig. 2a). Again, the binary compound formed by A(a) and AB(a) species has saturated the catalyst surface ($\vartheta_A + \vartheta_{AB} \cong 0.90$). Slightly above p'_{1B_2} (Fig. 4b), the surface is mostly covered by the binary compound ($\vartheta_A \cong 0.13$, while $\vartheta_B \cong 0.008$), but, contrary to the previous case of model M1, the for-

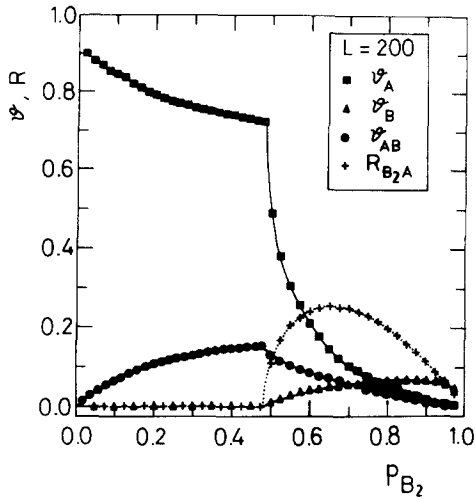

Fig. 3. Plot of the rate of B_2A production R and the surface coverages with the reactants versus p_{B_2} for model M2. Lattice size $L = 200$. More details in the text.

mation of $B(a)$ islands is prevented by B_2 desorption. Just when R becomes maximum, for $p_{B_2} \cong 0.65$ (Fig. 4c), most of the surface remains uncovered, i.e., $\vartheta_A \cong 0.16$, $\vartheta_{AB} \cong 0.07$, and $\vartheta_B \cong 0.04$. In this case $B(a)$ are the minority species, while $A(a)$ and $AB(a)$ species have a marked tendency to segregate into clusters. Lastly, for larger values of p_{B_2} ($p_{B_2} = 0.85$ in the example of Fig. 4d), $B(a)$ becomes the majority species on the surface with $\vartheta_B \cong 0.07$ as compared to $\vartheta_A \cong 0.03$ and $\vartheta_{AB} \cong 0.02$. So the major part of the catalyst surface remains uncovered and the reactants are rather scattered on the substratum mostly as monomers, dimers, and a few trimers.

The proposed reaction scheme for the DD process considers two competitive pathways (P1 and P2) leading to B_2A production, given by Eqs. (1e) and (1d), respectively. Therefore the Monte Carlo simulation provides the interesting possibility of monitoring the respective individual contributions to the rate of production, as shown in Figs. 5a and 5b for models M1 and M2, respectively. In the upper part of both figures the amount of B_2A obtained as a product of P1, $R(1)$, relative to the total production, $R(1+2)$, is plotted against p_{B_2}. The lower part of both figures shows the dependence on p_{B_2} of the total rate of B_2A production as well as the contribution of each pathway. In the case of model M1 one observes that $R(1)/R(1+2)$ decreases linearly within the whole reaction window when p_{B_2} is increased from p_{1B_2} to p_{2B_2} (Fig. 5a, upper part). This linear behavior is not observed for the case of model M2 (Fig. 5b, upper part).

For model M1 one has that close to p_{1B_2} (p_{2B_2}) the contribution of P1

(P2) is greater than that of P2 (P1), while close to $p_{B_2} \cong 0.5$ both contributions are equal. Consequently, $R(1)$ and $R(2)$ exhibit maxima at different values of p_{B_2} (more precisely, close to $p_{B_2} \cong 0.495$ and $p_{B_2} \cong 0.525$, respectively), while the maximum of $R(1+2)$ lies in between, close to $p_{B_2} \cong 0.51$ (Fig. 5a, lower part). These facts can be qualitatively understood by considering that, on the one hand, close to p_{1B_2} one has $\vartheta_{AB} > \vartheta_B$ and consequently P1 is favored, while on the other hand, close to p_{2B_2} one has $\vartheta_B \gg \vartheta_{AB}$ and therefore P2 is dominant. Summing up, for model M1 the total contribution of P2 within the whole reaction window is slightly greater than that of P1. Model M2 exhibits a similar behavior to model M1, as follows from the comparison of the lower parts of Figs. 5b and 5a, respectively. Nevertheless, for model M2 the total contributions of both P1 and P2 to the rate of B_2A production are approximately the same.

(a)

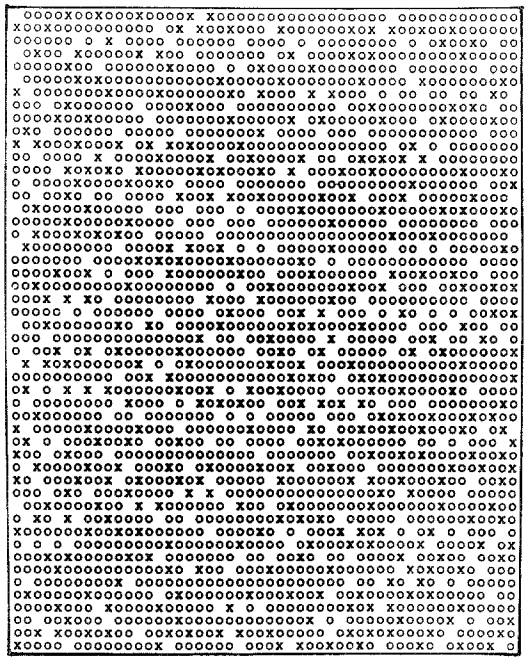

Fig. 4. Typical snapshot configurations of the reactants on the surface characteristic of the model M2. Sample size $L = 50$; (○) A(a), (■) B(a), and (×) AB(a), empty sites are left in white. (a) Saturated surface with A(a) ($\vartheta_A \cong 0.727$) and AB(a) ($\vartheta_{AB} \cong 0.15$) after $t = 2 \times 10^3$ for $p_{B_2} = 0.4745$, i.e., just at p_{1B_2}; (b) configuration obtained slightly above the critical point for $p_{B_2} = 0.50$ ($t = 3 \times 10^3$), $\vartheta_A \cong 0.511$, $\vartheta_B \cong 0.008$, and $\vartheta_{AB} \cong 0.130$; (c) configuration characteristic of the stationary regime just when R becomes maximum for $p_{B_2} = 0.65$, $\vartheta_A \cong 0.164$, $\vartheta_B \cong 0.043$, and $\vartheta_{AB} \cong 0.068$; and (d) configuration obtained for $t = 3 \times 10^3$ and $p_{B_2} = 0.85$, $\vartheta_A \cong 0.028$, $\vartheta_B \cong 0.068$, and $\vartheta_{AB} \cong 0.021$.

(b)

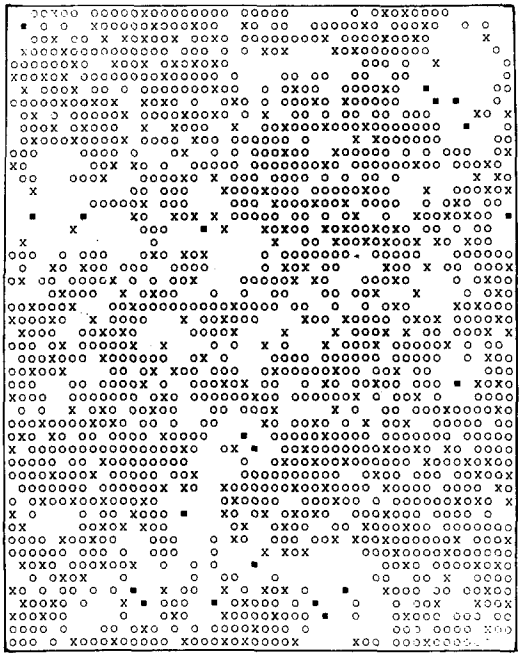

(c)

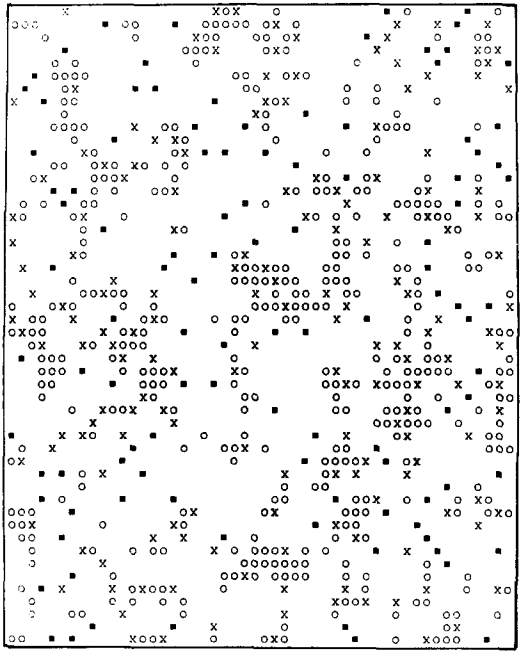

Fig. 4. (*Continued*)

(d)

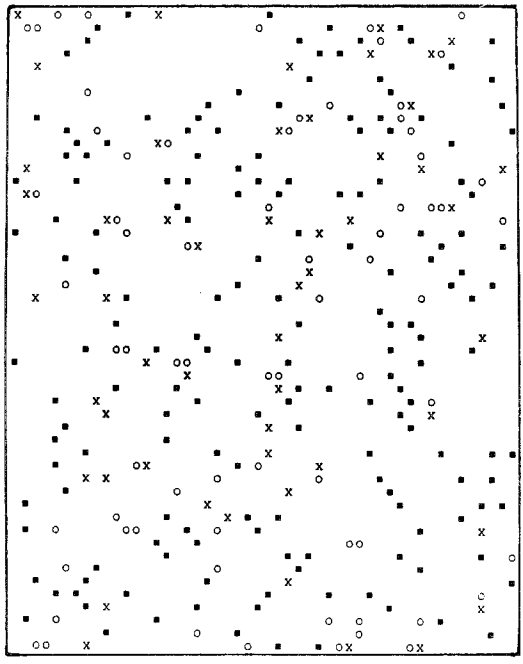

Fig. 4. (*Continued*)

After inspection of both Figs. 1 and 3 one observes that the studied quantities, namely R and the reactant's coverages, exhibit smooth variations close to the critical points. This fact indicates that the IPTs characteristic of the DD reaction scheme are of second order, in contrast to the DM reaction scheme, which shows first- and second-order IPT.[11-27]

Let us also note that, in contrast to the MM surface reaction scheme, which exhibits a trivial critical point with a "zero-width" reaction window,[4-10] both the DM[11-26] and the proposed DD model M1 surface reaction schemes exhibit "finite-width" reaction windows for $p_{B_2} < 1$. Nevertheless, the existence of this kind of interesting finite reaction window, which allows a detailed study of the critical behavior of the model (see Section 4.3), is due to quite different reasons in the two cases, i.e., the dimer requirement of two neighboring adsorption sites in the DM process and the recombination of AB(a) species in the DM model, respectively.

4.2. Determination of the Critical Points

In spite of the fact that the studied models have essentially a single parameter, namely p_{B_2}, some results may depend on the size of the lattice

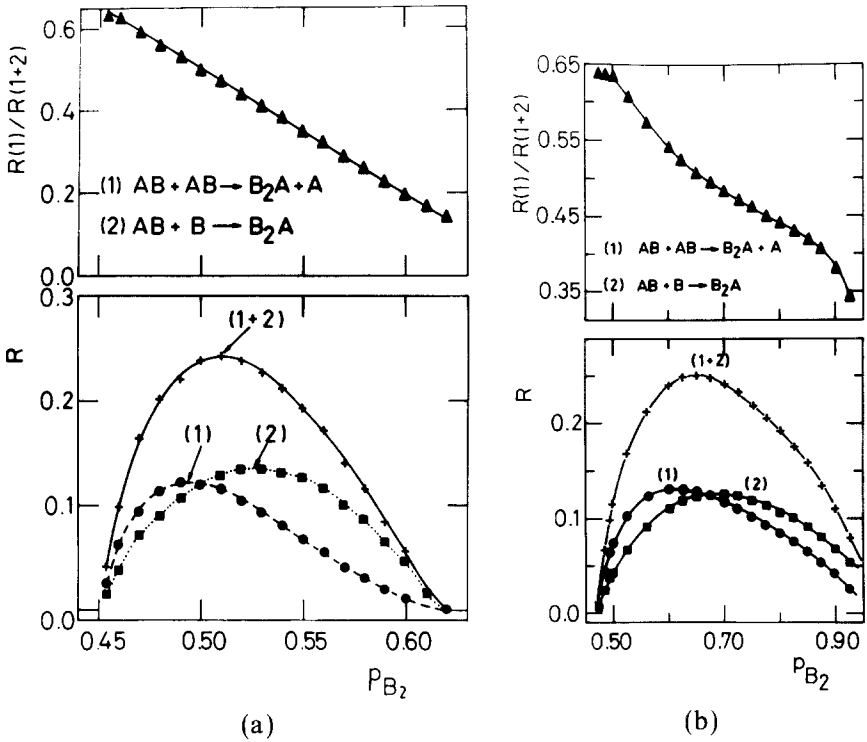

Fig. 5. Plots of the rate of production versus p_{B_2} within the stationary regime. Lower part: B_2A production due to step 1 (●) [i.e., Eq. (1e)], step 2 (■) [i.e., Eq. (1d)], and the total rate of production (+) due to both steps 1 and 2. Upper part: the rate of B_2A production due to step 1 relative to the total rate. (a) Model M1, (b) model M2.

employed in the simulation, so finite-size scaling analysis has to be applied. A phenomenological scaling approach for the treatment of IPTs based on well-established ideas of equilibrium phase transitions[44] has been proposed and successfully tested with Monte Carlo data obtained simulating the DM surface reaction process on incipient percolation clusters.[23] Here we only briefly describe the employed method.

During the stationary regime of the reaction (for $p_{1B_2} < p_{B_2} < p_{2B_2}$) it is assumed that the correlation length of clusters formed by the binary compound of $\{A(a) + AB(a)\}$ species [$B(a)$ clusters] adsorbed on the sample is $\xi_{A\text{-}AB}$ (ξ_B), respectively. Close to their respective critical points one expects that either $\xi_{A\text{-}AB}$ or ξ_B should grow and diverge in order to saturate the lattice, causing the reaction to stop. So, it is natural to assume that for $L = \infty$ the following behavior should hold:

$$\xi_i \propto |p_{B_2} - p_{jB_2}|^{-\nu_j}, \quad p_{B_2} \to p_{jB_2}, \quad i = \text{A–AB } (j=1),\ \text{B } (j=2) \qquad (2)$$

where v_j are the correlation length exponents. Nevertheless, working with finite lattices, the poisoning transitions are observed at L-dependent "critical probabilities" $p_{jB_2}(L) \neq p_{jB_2}$. This behavior can be understood by assuming that the poisoning of finite lattices occurs when the correlation length of the clusters formed by one of the reactants matches the lattice size, i.e., $\xi_i = L$. So, using Eq. (2), it follows that

$$p_{jB_2}(L) = p_{jB_2} + C_j L^{-w_j}, \qquad w_j = 1/v_j \tag{3}$$

where C_j are constants. Therefore, working with finite lattices of size L one obtains L-dependent "critical probabilities,"[22,23,28] say $p_{jB_2}(L)$ with $j = 1, 2$ and $p'_{1B_2}(L)$ for models M1 and M2, respectively, as usually happens when studying reversible phase transitions using the Monte Carlo method.[44] Then, using Eq. (3), it should be possible, in principle, to estimate both the critical points and w_j (or v_j).

In the present work L-dependent "critical probabilities" are obtained as follows: first, the poisoning (saturation) probability (PP), i.e., the number of trials in which the system poisons, is determined as a function of p_{B_2} for lattices of different size. The PP values are evaluated performing 10^2 Monte Carlo simulations with different samples up to a maximum time of $t = 10^4$. Then, the "critical points" $p_{jB_2}(L)$ are determined by taking the limit $\mathrm{PP} \to 0$ and assuming error bars given by the interval between consecutive data points. Even for rather small lattices this procedure is time-consuming, but this shortcoming can be avoided because one only needs to make a detailed scan of p_{B_2} values close to the limit $\mathrm{PP} \to 0$.

It should be noticed that the L-dependent "critical probabilities" would also depend on the particular conditions assumed for their determination, for example, performing a different number of Monte Carlo simulations or waiting for poisoning during a different period of time. Also, for a finite system with adsorbing (poisoned) states, these states may always be reached in the limit $t \to \infty$. Nevertheless, it is expected that this process may take a very long time[20] and consequently the PP is actually calculated for metastable states at some fixed long time ($t = 10^4$, in the present case), which is, however, still much shorter than their lifetime. So, for finite lattices and finite simulation time, one has that PP vanishes at some $p_{jB_2}(L)$, but for $L = \infty$ and $t = \infty$ it cannot precisely vanish. In spite of these shortcomings it seems that one gets reliable estimates for the $L \to \infty$ critical probabilities, while, on the other hand, one expects that they may be independent of the employed method.

Knowing the L-dependent "critical probabilities," we can use plots of the type $p_{jB_2}(L)$ versus L^{-w_j} to determine both the ordinate intercept given by $p_{jB_2}(L = \infty)$ and the extrapolation exponents w_j, as shown in Figs. 6

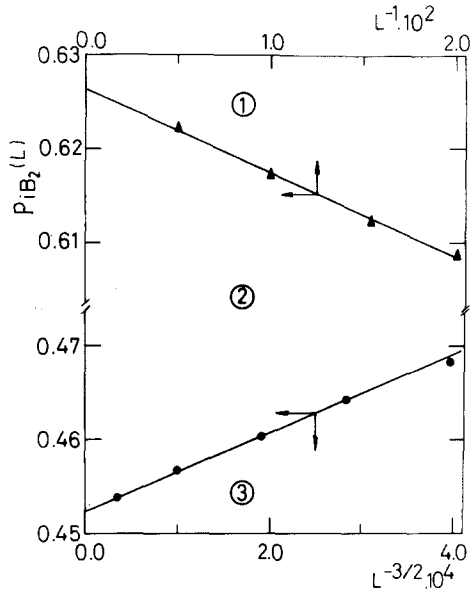

Fig. 6. The L-dependent critical probabilities $p_{iB_2}(L)$ plotted against L^{-w_i} $(i=1,2)$. In all cases the error bars are of the size of the point itself or smaller. The straight lines are the least-squares fits of the data, which intercept the vertical axis at the $L\to\infty$ critical probabilities given by $p_{1B_2}\cong 0.4525$ $(w_1=3/2)$ and $p_{2B_2}\cong 0.6263$ $(w_2=1)$, respectively. Within region (1) the surface becomes poisoned by B(a) species, region (2) corresponds to the stationary reactive regime and within region (3) the surface becomes saturated by A(a) and AB(a) species.

and 7 for models M1 and M2, respectively. In fact, for model M1 it is found that plots of $p_{1B_2}(L)$ versus $L^{-3/2}$ $(w_1=3/2)$ and $p_{2B_2}(L)$ versus L^{-1} $(w_2=1)$ give straight lines (Fig. 6) which intercept the ordinate at the critical points $p_{1B_2}(L=\infty)\cong 0.4525$ and $p_{2B_2}(L=\infty)\cong 0.6263$, respectively. Also, for model M2, a plot of $p'_{1B_2}(L)$ versus $L^{-3/2}$ $(w'_1=3/2)$ allow us to extrapolate the value $p'_{1B_2}(L=\infty)\cong 0.4745$ (Fig. 7). It should be noticed that this method is not particularly sensitive to the w_j exponent values, so plots like those shown in Figs. 6 and 7, which correspond to the best fits, are made assuming exact fractions or integer numbers for the exponents. Using this procedure, the error bars in the determination of the exponents are of the order of $\pm 15\%$. On the other hand, the critical points can be determined more accurately, i.e., within an error of about ± 0.0005.

It is interesting to note that at the critical points p_{1B_2} and p'_{1B_2} the surface coverage with A(a) species is within the range of critical probabilities p_c already determined for various percolation models in the square lattice given, for example, by $0.47\leqslant p_c\leqslant 0.66$[45–48]; however, for strong correlations (clustering), lattice percolation can become a continuum problem

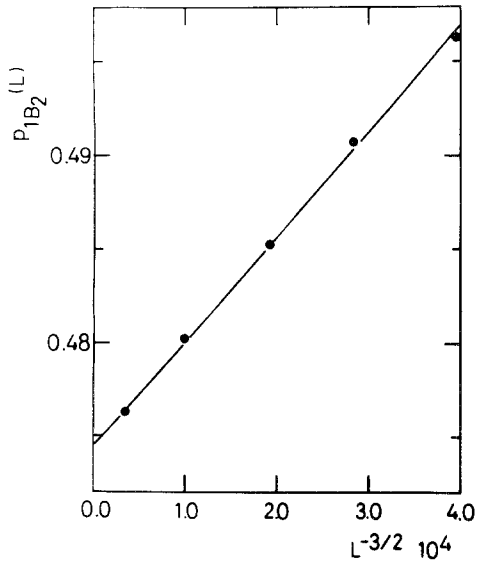

Fig. 7. The L-dependent critical probabilities $p_{1B_2}(L)$ plotted against $L^{-w_1'}$. In all cases the error bars are of the size of the point itself or smaller. The straight line is the least-squares fit of the data, which intercept the vertical axis at the $L \to \infty$ critical probability given by $p'_{1B_2} \cong 0.4745$ ($w_1' = 3/2$). Note that within the region above (below) the straight line the system exhibits a reactive stationary state [a saturated state with A(a) and AB(a) species].

where any p_c is possible (for reviews on percolation theory see ref. 49). So, one may consider, among others, the following two possibilities: (i) Both components of the binary compound are well mixed, preventing the formation of A(a) spanning clusters, or (ii) A(a) islands may span over the whole lattice, forming some sort of backbone to which AB(a) species (the minority) can be somewhat attached. These possibilities have been investigated and it is found that at the critical points one has spaning clusters of A(a) species, but they are homogeneous with fractal dimension $D = 2$ because, in both models, the formation of incipient percolation clusters takes place for p_{B_2} values greater than the critical points. This finding is in qualitative agreement with the snapshot configurations shown in Figs. 2a and 4a, but in contrast to the fractal clustering of reactants on the catalyst surface observed in simulations of the MM surface reaction process.[4]

Recently, Grinstein *et al.*[50] proposed that the second-order IPT of the DM surface reaction process belongs to the same universality class as Reggeon field theory (RFT),[51] which is also the same as that of directed percolation (DP) in $2+1$ dimensions.[52,53] This conjecture has very recently been confirmed by Jensen, Fogedby and Dickman,[54] who found

critical exponents related to the dynamic behavior of the DM process in excellent agreement with those reported for DP.[53] Furthermore, it has been proposed[55] that continuous transitions into an absorbing state, even involving an arbitrary number of chemical components,[50] should also belong to the same universality class; see also refs. 38 and 56 and references therein. Within this context, one may expect that the present models, which exhibit nonunique absorbing states, should depart from the DP universality class. In order to compare the correlation length exponents of models M1 and M2 and DP, one has to recall that DP in $2+1$ dimensions is an anisotropic problem with two correlation length exponents, i.e., $\nu_{\|} \cong 1.27$ in the so-called "time direction"[52] and $\nu_{\perp} \cong 0.735$ in the remaining two "spatial (isotropic) directions."[52] Therefore, only the latter is relevant for comparisons with results from IPTs in surface reaction processes. The obtained results for models M1 and M2 close to p_{1B_2}, $\nu_1 = 1/w_1 \cong 2/3 \pm 15\%$, are consistent, within the error bars, with $\nu_1 \cong \nu_{\perp}$. It should also be noted that the structural properties of the binary compound close to the critical point are expected to be isotropic. Obviously, the universality class cannot be assigned based on the evaluation of a single exponent, so further work will be necessary in this sense; in particular, the calculation of dynamic exponents[54] is expected to be more fruitful. On the other hand, for model M1 close to p_{2B_2} one has $\nu_2 = 1/w_2 \cong 1.0 \pm 15\% \gg \nu_{\perp}$. This result strongly suggests that the second-order IPT of model M1 close to p_{2B_2} does not belong to the universality class of DP or RFT.

4.3. Study of the Critical Behavior

As already established in the case of reversible transitions,[44] it is also interesting in the study of IPTs to investigate if the behavior of the relevant magnitudes of the system close to the critical points is dominated by critical exponents. In order to analyze this critical behavior, it is convenient to propose a power-law dependence of the properties, so for the rate of B_2A production and the coverage with $B(a)$ species one has

$$R \propto (p_{B_2} - p_{1B_2})^{\beta_1} \tag{4}$$

and

$$\vartheta_B \propto (p_{B_2} - p_{1B_2})^{\beta_2} \tag{5}$$

respectively, where β_1 and β_2 are critical exponents of model M1. Note that for model M2 the replacements $p_{1B_2} \to p'_{1B_2}$ and $\beta_j \to \beta'_j$ $(j = 1, 2)$ have to be made. Also, it is convenient to investigate the critical behavior of the total coverage with the binary compound of $A(a)$ and $AB(a)$ species, given

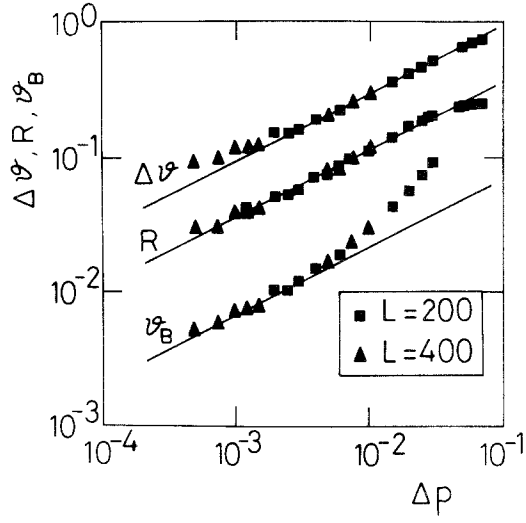

(a)

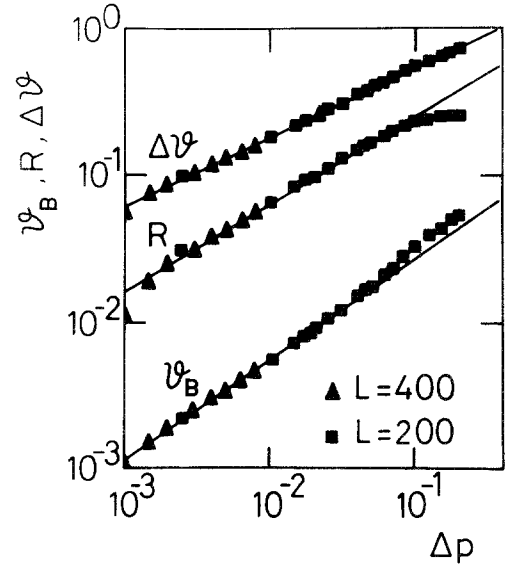

(b)

Fig. 8. (a) Log-log plot of $\Delta\vartheta$, R, and ϑ_B versus $\Delta p = p_{B_2} - p_{1B_2}$ [see Eqs. (4)–(6)] for model M1 and lattices of different size. The straight lines with slopes $\beta_i = 1/2$ ($i = 1, 2, 3$) have been drawn for comparison. (b) Same as in (a), but for model M2. The straight lines which have been drawn for comparison have slopes $\beta'_3 = 1/2$ (upper curve), $\beta'_1 = 3/5$ (middle curve), and $\beta'_2 = 2/3$ (lower curve).

by $\vartheta_{BC} = \vartheta_A + \vartheta_{AB}$. Since ϑ_{BC} is almost constant in the poisoned state and also practically equal, within error bars of about ± 0.01, to the occupancy probability ($p_0 \cong 0.907$[42,43]) of the random dimer filling problem, it is assumed that $\vartheta_{BC} \cong p_0$ also holds just at the critical point and in the $L \to \infty$ limit. So the proposed power-law dependence may be written as

$$\Delta\vartheta = (p_0 - \vartheta_{BC}) \propto (p_{B_2} - p_{1B_2})^{\beta_3} \tag{6}$$

where β_3 is also a critical exponent of model M1. The same assumption holds for model M2 but replacing p_{1B_2} and β_3 by p'_{1B_2} and β'_3, respectively.

In order to check the conjectured power-law behavior, Figs. 8a and 8b show plots of R, ϑ_B, and $\Delta\vartheta$ versus $\Delta p = p_{B_2} - p_{1B_2}$ for models M1 and M2, respectively. In all cases the obtained straight lines allow us to determine the critical exponents β_i and β'_i ($i = 1$–3), which are listed in Table I. In order to obtain reliable values for the critical exponents it is necessary on the one hand to work very close to the critical points, but on the other hand, to avoid the influence of finite-size effects, all data points in Fig. 8 are taken for p_{B_2} values greater than the L-dependent "critical probabilities." Obviously, the closer to the critical point one wants to work, the larger should be the lattice size employed in the simulation.

Since model M1 has another critical point at p_{2B_2}, a set of equations similar to Eqs. (2)–(4), capable of describing the critical behavior close to that point, also can be conjectured. For the sake of conciseness, let us denote by α_i ($i = 1,..., 4$) the critical exponents associated to R, $1 - \vartheta_B$, ϑ_A, and ϑ_{AB}, respectively. Note that all these quantities approach zero for $p_{B_2} \to p_{2B_2}$. Therefore, the study of the critical behavior of both models M1 and M2 involves the determination of ten critical exponents, which are listed in Table I. Figure 9 shows log-log plots of R, ϑ_A, ϑ_{AB}, and $1 - \vartheta_B$

Table I. Critical Points p_{iB_2} ($i = 1, 2$) Obtained for the $L = \infty$ Limit, the Extrapolation Exponents w_i ($i = 1, 2$), and Critical Exponents for Models M1 and M2[a]

Model M1	p_{1B_2}	w_1	β_1	β_2	β_3	
	0.4525	3/2	1/2	1/2	1/2	
	p_{2B_2}	w_2	α_1	α_2	α_3	α_4
	0.6263	1	2	2	2	2
Model M2	p'_{1B_2}	w'_1	β'_1	β'_2	β'_3	
	0.4745	3/2	3/5	2/3	1/2	

[a] Note that all exponents are approximated by exact fractions or integer numbers within an estimated error of about $\pm 15\%$ for w_j and $\pm 5\%$ or less for β_j, β'_j, and α_j. More details are given in the text.

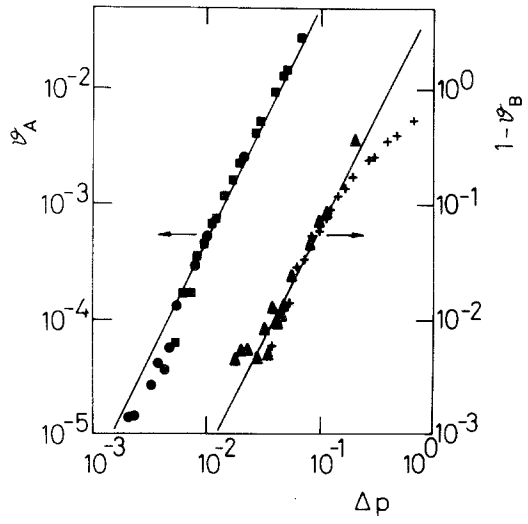

(a)

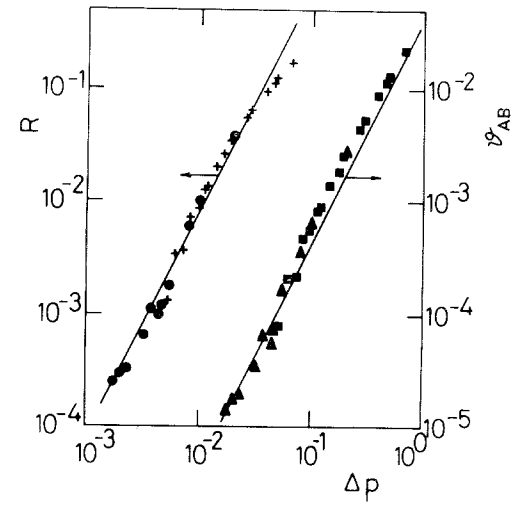

(b)

Fig. 9. (a) Log-log plot of (a) ϑ_A and $1-\vartheta_B$ and (b) R and ϑ_{AB} versus $\Delta p = p_{B_2} - p_{2B_2}$, respectively. Lattice size: (●, ▲) $L=400$, (■, +) $L=200$. Data corresponding to $1-\vartheta_B$ and ϑ_{AB} have been shifted one decade to the right for the sake of clarity in (a) and (b), respectively. The straight lines with slopes $\alpha_i = 2$ ($i = 1$–4) have been drawn for comparison.

versus $\Delta p = p_{2B_2} - p_{B_2}$ which allow us to determine the critical exponents α_i ($i = 1$–4).

As discussed above, let us note that an interesting open question is to determine the universality class of the DD surface reaction models which exhibit IPTs. Since the critical exponents (β_j and β_j') calculated for models M1 and M2 at the critical point of lower p_{B_2} value are different, one expects that these models belong to different universality classes. Furthermore, that change of the universality class is caused by B_2 desorption, which in fact is the only difference between the models.

5. CONCLUSIONS

Two models for the dimer–dimer surface reaction scheme of the type $(1/2)\,A_2 + B_2 \to B_2A$ which involves the formation of adsorbed AB intermediates have been proposed and discussed. Neglecting desorption of B_2 molecules (model M1), one observes two IPTs from a reactive state to two different off-equilibrium poisoned states with, on the one hand, a binary compound formed by A(a) and AB(a) species, and on the other hand a B(a)-saturated surface. Incorporating the desorption of B_2 molecules (model M2), the IPT from the reactive regime to the B(a)-saturated state is no longer observed. The critical values of the mole fraction of B_2 in the gas phase at which the IPTs of both models occur are obtained in the limit $L = \infty$ using a suitable extrapolation method. The critical exponents which dominate the rate of reaction and the coverage with the reactants at criticality are determined.

In view of the great interest in the IPTs occurring in the dimer–monomer surface reaction process, it is expected that the IPTs characteristic of the discussed dimer–dimer surface reaction schemes would stimulate further experimental and theoretical work in the field of kinetic transitions.

ACKNOWLEDGMENTS

This work was supported by the Consejo Nacional de Investigaciones Científicas y Técnicas (CONICET) de la República Argentina. The Alexander von Humboldt Foundation (Germany) is greatly acknowledged for the provision of valuable equipment.

REFERENCES

1. R. B. Anderson and P. T. Dawson, eds., *Experimental Methods in Catalytic Research* (Academic Press, New York, 1976).
2. C. H. Wu and E. W. Montroll, *J. Stat. Phys.* **30**:537 (1983).

3. L. W. Anacker, R. Kopelman, and J. S. Whitehouse, *J. Stat. Phys.* **36**:591 (1984); M. Silverberg and A. Ben-Shaul, *J. Stat. Phys.* **52**:1179 (1988).
4. R. M. Ziff and K. Fichthron, *Phys. Rev. B Rapid Commun.* **34**:2038 (1986).
5. A. Sadiq and K. Yaldram, *J. Phys. A Math. Gen.* **21**:L207 (1988).
6. K. Fichthron, E. Gulari, and R. M. Ziff, *Phys. Rev. Lett.* **63**:1527 (1989).
7. K. Fichthron, E. Gulari, and R. M. Ziff, *Chem. Ing. Sci.* **44**:1403 (1989).
8. M. A. Khan and K. Yaldram, *Surface Sci.* **219**:445 (1989).
9. D. ben-Avraham, S. Redner, D. Considine, and P. Meakin, *J. Phys. A Math. Gen.* **23**:L613 (1990).
10. D. ben-Avraham, D. Considine, P. Meakin, S. Redner, and H. Takayasu, *J. Phys. A Math. Gen.* **23**:4297 (1990).
11. R. M. Ziff, E. Gulari, and Y. Barshad, *Phys. Rev. Lett.* **56**:2553 (1986).
12. R. Dickman, *Phys. Rev. A* **34**:4246 (1986).
13. P. Meakin and D. J. Scalapino, *J. Chem. Phys.* **87**:731 (1987).
14. B. Chopard and M. Droz, *J. Phys. A Math. Gen.* **21**:205 (1988).
15. K. Yaldran and A. Sadiq, *J. Phys. A Math. Gen.* **22**:1925 (1989).
16. P. Fisher and U. M. Titulaer, *Surface Sci.* **221**:409 (1989).
17. M. Ehsasi, M. Matloch, O. Frank, J. H. Bloch, K. Chrismann, F. S. Rys, and W. Hirschwald, *J. Chem. Phys.* **91**:4949 (1989).
18. H. P. Kaukonen and R. M. Nieminen, *J. Chem. Phys.* **91**:4380 (1989).
19. I. Jensen and H. C. Fogedby, *Phys. Rev. A* **42**:1969 (1990).
20. D. Considine, H. Takayasu, and S. Redner, *J. Phys. A Math. Gen.* **23**:L1181 (1990).
21. M. Dumont, P. Dufour, B. Sente, and R. Dagonnier, *J. Catalysis* **122**:95 (1990).
22. E. V. Albano, *J. Phys. A Math. Gen.* **23**:L545 (1990).
23. E. V. Albano, *Phys. Rev. B Rapid Commun.* **42**:10818 (1990).
24. E. V. Albano, *Surface Sci.* **235**:351 (1990).
25. E. V. Albano, *J. Chem. Phys.* **94**:1499 (1991).
26. J. W. Evans and M. S. Miesch, *Phys. Rev. Lett.* **66**:833 (1991).
27. J. W. Evans and M. S. Miesch, *Surface Sci.* **245**:401 (1991).
28. E. V. Albano, to be published.
29. M. Faraday, *Experimental Researches in Electricity* (London, 1844).
30. P. R. Norton, in *Chemical Physics of Solid Surfaces and Heterogeneous Catalysis*, Vol. 4, D. A. King and D. P. Wooddruff, eds. (Elsevier, Amsterdam, 1982), p. 27.
31. B. E. Nieuwenhys, *Surface Sci.* **126**:307 (1983).
32. B. Helling, B. Kasemo, S. Ljungström, A. Rosén, and T. Wahnström, *Surface Sci.* **189/90**:851 (1987).
33. S. Ljungström, B. Kasemo, A. Rosén, T. Wahnström, and E. Fridell, *Surface Sci.* **216**:63 (1989).
34. T. Wahnström, E. Fridell, S. Ljungström, B. Helling, B. Kasemo, and A. Rosén, *Surface Sci.* **223**:L905 (1989).
35. H. Yang and J. L. Whitten, *Surface Sci.* **223**:131 (1989).
36. E. V. Albano, *J. Phys. A Math. Gen.* **25**:2557 (1992).
37. E. V. Albano, *Appl. Phys. A* (1992), in press.
38. J. W. Evans, *Langmuir* **7**:2514 (1991).
39. G. Jones and M. Goldsmith, in *Programming in OCCAM 2*, C. A. R. Hoare, ed. (Prentice-Hall International, London, 1988).
40. W. Paul, D. W. Heermann, and R. C. Desai, *J. Comp. Phys.* **82**:489 (1989).
41. E. V. Albano, K. Binder, D. Heermann, and W. Paul, *J. Stat. Phys.* **61**:161 (1990).
42. J. W. Evans, D. R. Burgess, and D. K. Hoffman, *J. Chem. Phys.* **79**:5011 (1983).
43. J. W. Evans and R. S. Nord, *Phys. Rev. B* **31**:1759 (1985); R. S. Nord and J. W. Evans, *J. Chem. Phys.* **93**:8397 (1990).

44. K. Binder, ed., *Monte Carlo Methods in Statistical Physics* (Springer, Berlin, 1979).
45. H. O. Mártin, E. V. Albano, and A. Maltz, *J. Phys. A Math. Gen.* **20**:1531 (1987).
46. E. V. Albano and H. O. Mártin, *Thin Solid Films* **151**:121 (1987).
47. H. O. Mártin and E. V. Albano, *Z. Phys. B* **70**:213 (1988).
48. S. R. Anderson and F. Family, *Phys. Rev. A* **38**:4198 (1988).
49. D. Stauffer, *Introduction to the Percolation Theory* (Taylor and Francis, London, 1985).
50. G. Grinstein, Z. W. Lai, and D. A. Browne, *Phys. Rev. A* **40**:4820 (1989).
51. P. Grassberger and A. de la Torre, *Ann. Phys.* (N.Y.) **122**:373 (1979).
52. Wolfgang Kinzel, Directed percolation, in *Percolation Structures and Processes*, G. Deutscher, R. Zallen, and J. Adler, eds. (Israel Physical Society, Jerusalem, 1983), Chapter 18.
53. P. Grassberger, *J. Phys. A Math. Gen.* **22**:3673 (1989).
54. I. Jensen, H. C. Fogedby, and R. Dickman, *Phys. Rev. A* **41**:3411 (1990).
55. P. Grassberger, *Z. Phys. B* **47**:365 (1982).
56. R. Dickman, *Phys. Rev. A* **40**:7005 (1989).